Refinement and application of a modified indentation toughness technique

Robert F. Cook
Winterville, NC 28590
USA
robertfcook@mac.com

The modified indentation toughness technique, in which indentation strength and crack length at instability are combined in toughness determination, is re-assessed by addition of new data and materials, including those of other investigators. A materials ranking scheme is introduced and the technique extended in determination of the variation in toughness with crack length for T curve materials. In all, 20 materials are assessed here to refine the precision and accuracy of the technique and enable toughness estimation for ceramics at strength relevant length scales. Artifacts associated with conventional indentation toughness methods are largely removed by the modified technique.

Cite as
Cook, Robert F. (2020, September 18). Refinement and application of a modified indentation toughness technique (Version 1.0). Zenodo. http://doi.org/10.5281/zenodo.4036754

1. INTRODUCTION

The load-bearing performance and reliability of structural ceramic components often depends on the fracture behavior of small flaws. Such flaws are frequently comparable in scale to the ceramic microstructure and consist of cracks associated with pores, inclusions, large grains in polycrystals, or sharp contacts on surfaces. Fracture behavior is determined qualitatively by three factors: (i) the nature of the global loading on the component, *e.g.*, tensile stress generated by thermal shock or by mechanical bending; (ii) the nature of the flaw, including crack geometry and any stress fields locally surrounding the flaw; and (iii) the fracture resistance or toughness characteristics of the ceramic, particularly any variations in toughness at the scale of the flaw. In quantitative fracture mechanics terms, the crack driving force arising from the global loading and local stress field can be expressed functionally as a crack length dependent stress-intensity factor (SIF), $K(c)$, where c is a defined crack length. The crack resistance force, originating in the ceramic bonding and microstructure, is quantified by the toughness, $T(c)$. Fracture equilibrium is given by equating the driving force and the resisting force, $K(c) = T(c)$, making clear that fracture behavior is determined by influences associated with applied loading, $K(c)$, separate from those associated with the material, $T(c)$. Hence, the fracture properties of ceramic *materials* are most easily made by comparing toughness values. In particular, measurements of toughness at the small length scales associated with strength-controlling cracks and flaws are required to optimize and predict ceramic component load-bearing behavior. Such behavior dictates the performance of ceramic components in diverse applications such as displays in hand-held devices, substrates in automotive microelectronic applications, catalytic particles in chemical reactors, and armor plates to protect people, vehicles, and buildings.

The most common method of assessing toughness of ceramics at small length scales is by indentation crack length measurement [Anstis *et al.*, 1981]. In this method, a Vickers diamond pyramid is first brought into contact with a ceramic surface in a controlled load-unload cycle. The surface traces of the resulting indentation cracks are then measured and a simple calibrated power law formulation involving the crack lengths and the peak indentation load can be used to estimate the toughness. The major issues with this technique are that the calibration assumes that

the test environment is inert and that the residual stress field surrounding the contact is well characterized by the ceramic indentation hardness and elastic modulus. Both assumptions lead to inaccuracy, and to a lesser extent, imprecision, in toughness measurement. However, a recent extensive overview of indentation crack length measurements in air—overwhelmingly the most common ceramic fracture test—shows that such tests, although not calibrated toughness measurements, can be used to quantitatively rank ceramic cracking susceptibility [Cook, 2020], partially side-stepping environment and residual stress field concerns. A step closer to ceramic toughness measurement at small scales is the two step indentation-strength method [Chantikul *et al*., 1981]. In this method, a controlled indentation flaw is introduced into a ceramic test component as above. The strength of the component is then measured under inert conditions and another calibrated power law formulation involving the strength and the indentation load used to estimate the toughness. Although there are sometimes test environment concerns, there is a much weaker dependence on the nature of the residual field, and toughness measurement by this technique can be quite accurate and precise. Extensions to the technique, quantifying the effects on strength and toughness of multi-scale environmental, microstructural, and geometrical influences, have been demonstrated [Cook, 2015].

Here, the attributes of both indentation tests above are combined into a modified indentation toughness technique that almost completely removes residual stress field effects from toughness assessment. Indentation crack lengths are still measured, but *after* inert strength testing of components. The post test crack lengths are combined with the strengths to generate a parameter that is directly proportional to the toughness through the crack geometry alone. The convenience of indentation testing is retained in that the scale and location of the strength-controlling flaw are determined by the experimenter. The modified technique was demonstrated in an earlier work [Cook and Lawn, 1983] but involved limited materials and measurements. Here, the technique is revisited with a wider domain of materials and ensuing range of data, including materials in which microstructural effects on toughness are evident and including data from other investigators. In addition, the results of the modified technique are placed in the context of the more recent crack length and strength measurement works [Cook, 2015, 2020] and pursues the philosophy of the recent considerations regarding indentation crack lengths in air [Cook, 2020]

to generate a quantitative ranking scheme for ceramic fracture susceptibility. The work here begins with an overview of the required analysis and experimental method. The results section then follows in three parts: a comparison with conventional test methods; a refinement of the modified technique; and, application of the modified technique to ceramics exhibiting microstructural effects on toughness. A discussion compares the refined modified technique to short and long crack toughness measurement methods.

2. METHODS

2.1. Analysis

Analytical development begins with consideration of equilibrium indentation crack lengths in materials with single valued toughness. In inert conditions, the right side of the equilibrium equation above is then $T(c) = T_0$, where T_0 is the material toughness in inert conditions and the "0" subscript indicates no chemical reactions between the material and the environment. For a crack under the sole influence of the indentation residual field, the left side of the equilibrium equation is the SIF $K(c) = \chi_0 P/c^{3/2}$, where the crack length c is measured from the center of the indentation, P is the peak indentation load, and χ_0 is a dimensionless geometry factor appropriate to indentation in an inert environment. Combining these two expressions gives the inert indentation crack length,

$$c_0 = (\chi_0 P/T_0)^{2/3}. \quad (1)$$

Under the more common conditions of indentation in air, the right side of the equilibrium equation is $T(c) = T_{\text{air}}$, where T_{air} is the toughness in air, recognizing that most ceramic materials, especially those containing oxygen, react with atmospheric moisture, such that $T_{\text{air}} < T_0$ for an equilibrium crack in the reactive air. The left side of the equilibrium equation is now $K(c) = \chi_{\text{air}} P/c^{3/2}$, where χ_{air} is the dimensionless geometry factor appropriate to indentations in air, recognizing that for most such indentations, especially those at large loads, secondary lateral cracks and chips form, relaxing the residual field such that $\chi_{\text{air}} < \chi_0$. Combining these latter two expressions gives the equilibrium indentation crack length in air,

$$c_{\text{air}} = (\chi_{\text{air}} P / T_{\text{air}})^{2/3}. \tag{2}$$

For most ceramics, $T_{\text{air}}/T_0 < \chi_{\text{air}}/\chi_0$, such that indentation cracks in air are longer than those in inert conditions, $c_{\text{air}} > c_0$. Equation (1) was the basis for the original indentation crack length toughness estimation method, calibrating χ_0 by measurements on materials of known hardness, modulus, and toughness [Anstis *et al.*, 1981]. In the recent overview of indentation crack lengths in air [Cook, 2020], Eq. (2) was the basis for materials fracture susceptibility comparisons using the load-adjusted crack length $c_{\text{air}} P^{-2/3}$, noting that this quantity is invariant for ideal indentations.

A uniform applied stress σ_{a} superposed on the indentation crack adds an additional SIF term $K = \psi \sigma_{\text{a}} c^{1/2}$, where ψ is another dimensionless geometry. factor, characterizing the effect of the applied stress on the crack. The equilibrium equation for an indentation crack formed in air and subsequently stressed in inert conditions is then

$$K(c) = \chi_{\text{air}} P / c^{3/2} + \psi \sigma_{\text{a}} c^{1/2} = T_0 \tag{3}$$

The maximum stress, σ_{m}, sustainable by the indentation flaw is given by simultaneous solution of Eq. (3) and the instability condition, $\mathrm{d}K(c)/\mathrm{d}c = 0$, such that

$$\sigma_{\text{m}} = 3T_0 / 4\psi c_{\text{m}}^{1/2}, \tag{4}$$

where

$$c_{\text{m}} = (4\chi_{\text{air}} P / T_0)^{2/3}. \tag{5}$$

The stress σ_{m} is the inert strength of the indented component. The conjugate crack length c_{m} characterizes the instability configuration and reflects near-equilibrium extension of the indentation crack from c_{air} to c_{m} under the action of the applied stress. Combining Eqs. (4) and (5) to eliminate c_{m} gives $\sigma_{\text{m}} = 3T_0^{4/3} / 4^{4/3} \psi \chi_{\text{air}}^{1/3} P^{1/3}$ and this is the basis for indentation-strength toughness estimation methods [Chantikul *et al.*, 1981; Cook, 2015], calibrating the product $\psi \chi_{\text{air}}^{1/3}$ by measurements on materials with known properties. It is noted that $\sigma_{\text{m}} P^{1/3}$ and $c_{\text{m}} P^{-2/3}$ are load adjusted inert instability parameters that are invariant for ideal indentations.

The dependence of inferred toughness on the indentation residual field characterized by χ is reduced in strength measurements relative to crack length measurements by the introduction of the SIF associated with the applied stress: $T_0 \sim \chi$ (crack length); $T_0 \sim \psi^{3/4} \chi^{1/4}$ (strength) [Anstis

et al., 1981; Chantikul *et al*., 1981]. The modified indentation toughness technique eliminates this dependence completely, as noted by re-arranging Eq. (4) to give

$$T_0 = (4\psi/3)\sigma_m c_m^{1/2}. \quad (6)$$

Toughness inferred from $\sigma_m c_m^{1/2}$, combined strength-crack length measurements, thus depends entirely on the applied stress related crack geometry factor: $T_0 \sim \psi$ (modified) [Cook and Lawn, 1983]. It is useful to compare the similarities and differences of Eq. (6) with equations used in toughness determinations using long crack "standard fracture mechanics specimens" (*e.g*., the double cantilever beam) [Murakami, 1987]. The major similarity is that in both cases toughness is determined by a product of the peak load or stress supported by the specimen and the crack length at fracture instability, mediated by a crack geometry term. The major difference is that fracture systems of long crack specimens are usually mechanically unstable, such that fracture instability occurs at peak load with no extension of the crack from an initial length. In contrast, fracture systems for indentation specimens pass from an initial stable configuration, Eq. (2), to an unstable configuration at peak load, Eq. (5), with attendant crack extension. A minor difference is that the geometry term for long crack specimens is usually a function of the initial crack length relative to the specimen dimensions, whereas this is not so in strength tests. Hence, the modified indentation toughness test fits within a recognized toughness measurement framework and combines the ease of indentation crack formation at strength-relevant length scales while by-passing the difficulties associated with significant residual stress field dependence. (Elastic-plastic deformation effects associated with the residual stress field exert geometrical influences on crack formation during the indentation cycle [Cook, 2019], but these cause secondary post-indentation effects.)

2.2. Experiment

The experimental technique for simultaneous determination of inert strength and instability crack length, and thus $\sigma_m c_m^{1/2}$, was primarily the dummy indentation method used earlier [Dabbs *et al*., 1982; Cook and Lawn, 1983]. Briefly, three co-linear indentations, formed at the same peak load and visually adjudged alike, were generated in air within the central spans of four-point bend

specimens of several ceramics and glasses, Fig. 1. The specimens were subsequently loaded to failure under inert conditions of flowing dry N_2 gas and rapid loading rate—the gas environment and the resulting short failure times, about 30 ms, minimized diffusion of moisture to the cracks during failure. Failure loads were recorded using a piezoelectric load cell and converted to failure stress using specimen and bend rig dimensions. The failure stresses were consistent with specimens containing single indentations and were thus regarded as σ_m measurements. The indentation loads were selected such that the specimens failed from one of the indentations on a plane perpendicular to the bending direction, Fig. 1(a). The cracks on the remaining, "dummy," indentations were measured after failure using a variety of optical microscopy techniques [Cook, 2020] and compared with measurements of indentation cracks on unstressed specimens. The cracks parallel to the failure plane exhibited significant extension and diminished opening while the cracks perpendicular to the failure plane exhibited no significant alteration, Fig. 1(b). As all indentations experienced the same stress history up to the inert strength, the lengths of the extended cracks were regarded as c_m estimates, Fig. 1(c).

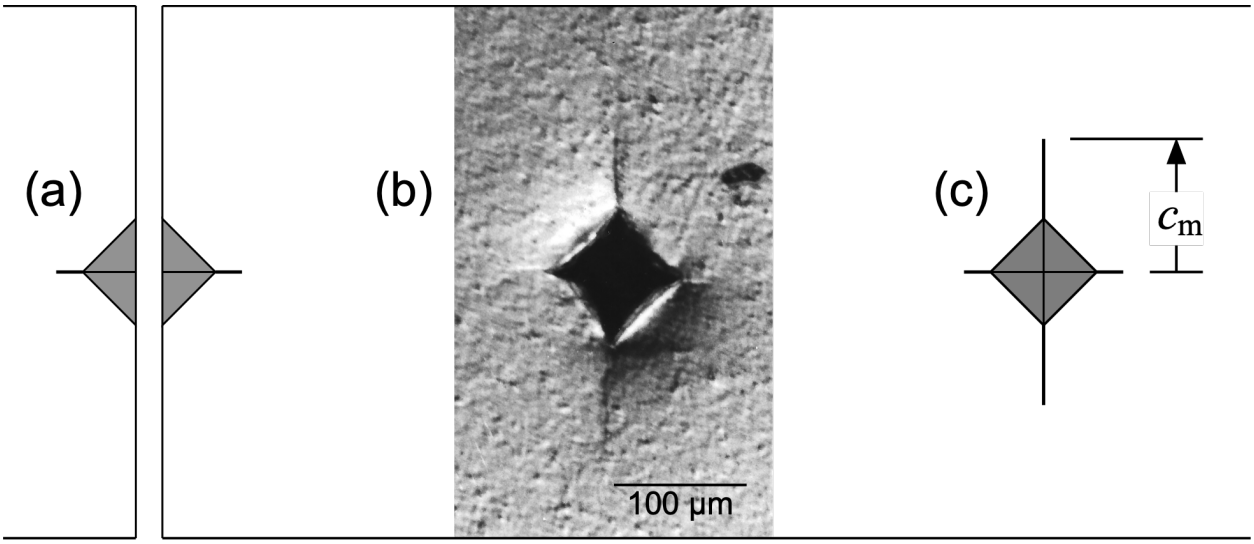

FIGURE 1 Schematic diagram and image of dummy indentation method used for determination of instability crack lengths: central span of bend specimen containing three identical indentations (bending induced tensile stress is horizontal). (a) Failure location, with failure plane extending across specimen. (b) Optical micrograph of GC1 ceramic with 20 N indentation and cracks extended perpendicular to stress. (c) Intact indentation with extended crack length indicated.

Using the above technique the $\sigma_m c_m^{1/2}$ data set used in the earlier work [Cook and Lawn, 1983] has been extended here by further measurements on additional specimens and additional materials, and, where possible, by analyzing all data using individual specimen σ_m-c_m pairs (rather than grouped data as earlier). The data were further extended by including comparable inert strength and crack length data obtained by other workers. Dummy technique measurements on silicon nitride, whisker reinforced alumina, and zirconia [Ramachandran and Shetty, 1991; Li *et al*., 1997] using rapid strength measurements in air are included. Direct observation measurements on silicon nitride, silicon, and alumina [Marshall, 1983; Cook, 2006; Braun *et al*., 1992] are also included. In the first two of these direct observation studies, the materials do not react with atmospheric moisture, and in the third study, inert conditions were obtained by indentation immersion in dry silicone oil. The data from other workers was obtained by digitizing and re-analyzing published results.

In all, data are included from 20 materials involving over 300 measurements of indentation instability configurations as well as related measurements of initial configurations. The materials included glasses, glass-ceramics, polycrystalline ceramics, and a single crystal and are listed by materials class in Table 1, along with ID codes for ease of notation, the sources of the materials and the data, and the techniques used to determine the modified toughness parameters (the ID codes are different from those used previously [Cook, 2020]). The data are reported as the mean values of $c_{air}P^{-2/3}$, $c_m P^{-2/3}$, $\sigma_m P^{1/3}$, and $\sigma_m c_m^{1/2}$ with uncertainties specified as experimental standard deviation limits, using propagation of variance as required. In addition, combining Eqs. (2) and (5) provides the relative crack extension

$$c_m/c_{air} = (4T_{air}/T_0)^{2/3}. \tag{7}$$

The implications of this equation are many-fold: First, the experimentally determined ratio c_m/c_{air} must be greater than 1 to verify stable crack extension during applied stressing to failure. Second, a lower bound toughness ratio required to generate such precursor extension is $T_{air}/T_0 \geq 0.25$; this criterion is usually easily met for ceramics reacting with moist air. Third an upper bound to the relative extension is $4^{2/3} \simeq 2.52$ for no reaction, $T_{air}/T_0 = 1$. As the bounds are fixed, the median value and range of c_m/c_{air} are reported.

Table 1 Ceramic materials included in modified toughness investigation

ID	Material	Data	Technique
SLG	Soda-lime silicate glass (Schott-Ruhrglas, Germany)	Dabbs, 1982	Dummy, N_2
BSG	Borosilicate glass (Schott-Ruhrglas, Germany)	Dabbs, 1982	Dummy, N_2
FS	Fused silica (Schott-Ruhrglas, Germany)	Dabbs, 1984	Dummy, N_2
GC1	Cordierite glass ceramic (Pyroceram C9606, Corning, Corning, NY)	Cook, 1982	Dummy, N_2
GC2	Li_2SiO_3 glass ceramic (Custom, 1.19 μm [Cook *et al.*, 1986])	This work	Dummy, N_2
GC3	Li_2SiO_3 glass ceramic (Custom, 1.90 μm [Cook *et al.*, 1986])	This work	Dummy, N_2
GC4	Li_2SiO_3 glass ceramic (Custom, 2.30 μm [Cook *et al.*, 1986])	This work	Dummy, N_2
PZT	(Pb, Zr)TiO_3 polycrystal (Plessey, Australia)	This work	Dummy, N_2
BT	$BaTiO_3$ polycrystal (Channel Industries, Santa Barbara, CA)	This work	Dummy, N_2
SYN	Synthetic rock (Synroc B, Australian Atomic Energy Establishment)	This work	Dummy, N_2
A1	Al_2O_3 polycrystal (AD96, Coors, Golden, CO)	This work	Dummy, N_2
A2	Al_2O_3 polycrystal (F99, Friedrichsfeld, Mannheim, Germany)	This work	Dummy, N_2
A3	Al_2O_3 polycrystal (Custom, 2.5 μm [Chantikul *et al.*, 1990])	Braun, 1992	Direct, oil
AS	Al_2O_3-SiC (whisker) composite (Ceramatec Inc., Salt Lake City, UT)	Ramachandran, 1991	Dummy, air
AT	Al_2O_3-Al_2TiO_5 composite (Custom [Bennison *et al.*, 1991])	Braun, 1992	Direct, oil
TZP	3 mol % Y_2O_3-ZrO_2 polycrystal (Tosoh Corporation, Tokyo, Japan)	Li, 1997	Dummy, air
SC	SiC polycrystal (NC203, Norton Co., Worcester, MA)	This work	Dummy, N_2
SN1	Si_3N_4 polycrystal (NC132, Norton Co., Worcester, MA)	Marshall, 1983	Direct, air
SN2	Si_3N_4 polycrystal (SN252, Kyocera, Des Plaines, IL)	Ramachandran, 1991	Dummy, air
Si	(001) single crystal Si	Cook, 2006	Direct, air

3. RESULTS

3.1. Relation to conventional method

Figure 2 is a plot of the initial and final indentation crack lengths for the complete materials set examined here, plotted using load-adjusted coordinates $c_{\text{air}}P^{-2/3}$ and $c_{\text{m}}P^{-2/3}$, respectively. The plotting scheme is the same as that used in the recent review of indentation crack lengths in air [Cook, 2020], ranking the materials left to right by increasing $c_{\text{air}}P^{-2/3}$ value. The gray band in Fig. 2 represents the range of $c_{\text{air}}P^{-2/3}$ responses from the review for a similarly broad set of ceramic materials (some representative materials are in common, *e.g.*, SC, A1, SLG). The lower group of small open symbols in Fig. 2 represents the $c_{\text{air}}P^{-2/3}$ responses for the set of materials examined here. There is close agreement with the range of the previous observations and with the ranking of materials by susceptibility to indentation cracking. Ceramics regarded as "tough," *e.g.*, SC, SN series, appear on the left of the plot, ceramics regarded as "not very tough," *e.g.*, SLG, Si, appear on the right side of the plot, and families of materials, *e.g.*, A series, GC series are clustered together. The major ranking irregularity in this scheme is that the "anomalous" glasses, FS and BSG, are not clustered with SLG, and in fact appear in the center of the ranking, implying a much greater toughness. The origin of this observation is that χ is depressed for these materials, leading to shorter than expected crack lengths, Eq. (2). Overcoming this effect was a major factor in the initial development of the modified toughness technique [Cook and Lawn, 1983].

The upper group of large, solid symbols in Fig. 2 represents $c_{\text{m}}P^{-2/3}$ responses for the majority of materials examined here. These materials were judged to exhibit load-invariant indentation behavior and are considered here first. The indentation loads used, the number of cracks measured, and the resulting $c_{\text{m}}P^{-2/3}$ mean values and uncertainties are given in Table 2. In all cases $c_{\text{m}}P^{-2/3} > c_{\text{air}}P^{-2/3}$, indicating that precursor crack extension occurred during loading and that interpretation of the instability data in ideal indentation terms, Eqs. (1)–(6), was applicable. In a few cases, notably the SN1 and A3 materials, the relative precursor extension approached the upper bound, $\simeq 2.5$. In most materials, the precursor extension was much less

than this, in fact the lower bound for $c_m/c_{air}$was 1.2 and the median extension was 1.34, implying $T_{air}/T_0 \simeq 0.39$ for these materials (this small value is discussed below). The trend in increasing $c_m P^{-2/3}$ is similar to that for $c_{air}P^{-2/3}$, although it is clear that the detailed ranking would change if cracking susceptibility $c_m P^{-2/3}$ were used rather than $c_{air}P^{-2/3}$.

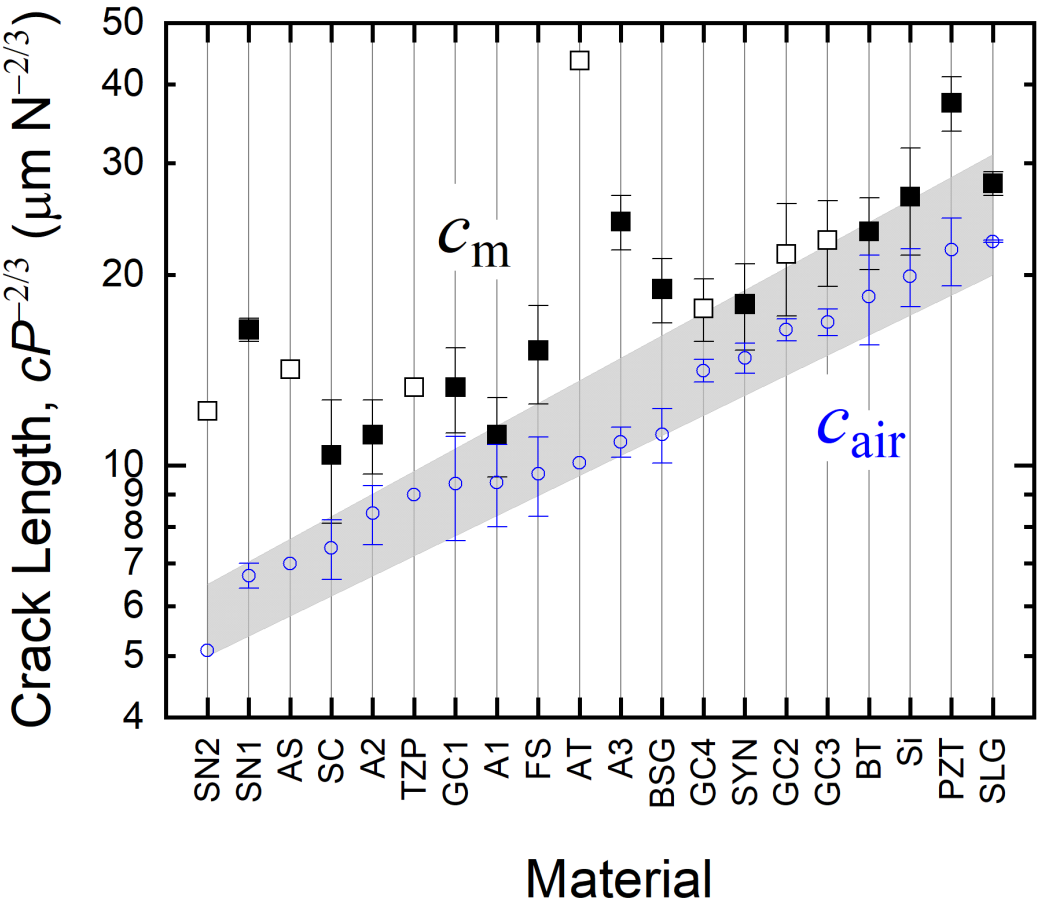

FIGURE 2 Plot of load adjusted crack length for ceramic materials containing indentations in air, c_{air}, and at instability under applied stress in inert conditions, c_m. Shaded band indicates range of responses from review of conventional, air-based, measurements.

The large open symbols in Fig. 2 represent $c_m P^{-2/3}$ responses of materials that exhibited load-dependent indentation behavior: the responses shown were measured at the largest load applied. These loads are given in Table 2, along with the measured $c_m P^{-2/3}$ values and uncertainties where applicable; the loads and measurements are indicated by an asterisk (*). In

many cases, load-dependent responses at indentation instability are an indication of significant microstructural effects giving rise to an increasing toughness with crack length—a T curve, $T(c)$ [Cook, 2015]. Such toughness increases lead to enhanced stability of a fracture system and elongated stable extension of cracks prior to instability and failure under applied stress. An example of elongated extension is noted for the AT material that was deliberately engineered for microstructural influence leading to a T curve [Bennison, 1991]. Other materials that exhibited load-dependent behavior and that are regarded as toughened include the whisker-reinforced AS material and the phase transforming TZP material. The $T(c)$ variations determined from application of the modified indentation toughness technique to the complete data sets for the open symbol materials are considered in section 3.3.

3.2. Refinement of modified technique

Figure 3 is plot of the indentation instability parameter $\sigma_m c_m^{1/2}$ for the complete materials set examined here. The figure uses a plotting scheme similar to that in Fig. 2, ranking materials from left to right in order of increasing $\sigma_m c_m^{1/2}$ value. The filled symbols represent the mean values and standard deviation limits for $\sigma_m c_m^{1/2}$ determined in most cases by analyzing individual σ_m-c_m pairs. In a few cases, *e.g.*, SLG, the means and standard deviations of grouped $\sigma_m P^{1/3}$ and $c_m P^{-2/3}$ values for a material were used to determine the mean $\sigma_m c_m^{1/2}$ values and standard deviation limits were determined by analysis of variance. For all materials, the number of strengths measured, if different from the number of cracks, and the resulting $\sigma_m P^{1/3}$ mean values and uncertainties are given in Table 2. As in Fig. 2, the open symbols in Fig. 3 represent the large load $\sigma_m c_m^{1/2}$ responses of materials that exhibited load-dependent indentation behavior. The strength values used are given in Table 2 with uncertainties where applicable; the strengths are indicated by an asterisk (*). For all materials, the values, and uncertainties where applicable, for $\sigma_m c_m^{1/2}$ are given in Table 2, ranked as in Fig. 3.

There are many points to note in Fig. 3. First, the $\sigma_m c_m^{1/2}$ values are comparable to the accepted long crack toughness values: The toughness of Si and glasses is approximately 0.7 MPa $m^{1/2}$, the toughness of polycrystalline alumina is approximately 2 MPa $m^{1/2}$, and the toughness of

microstructurally engineered materials that are toughened by crack-front transformation processes (TZP) or crack-wake traction zones (AS, AT) often exceeds 5 MPa $m^{1/2}$. The implication is that the geometrical factor for indentation flaws under applied stress $(4\psi/3) \simeq 1$, Eq. (6). Second, the $\sigma_m c_m^{1/2}$ values for the glasses, SLG, BSG, and FS, are identical within experimental uncertainty. The artifact of separation arising from crack length or strength measurements alone (Table 2) is removed. Third, the relative measurement uncertainty for all materials is small: the standard deviation/mean ratio is approximately ± 8 %, independent of the value of $\sigma_m c_m^{1/2}$ and the material.

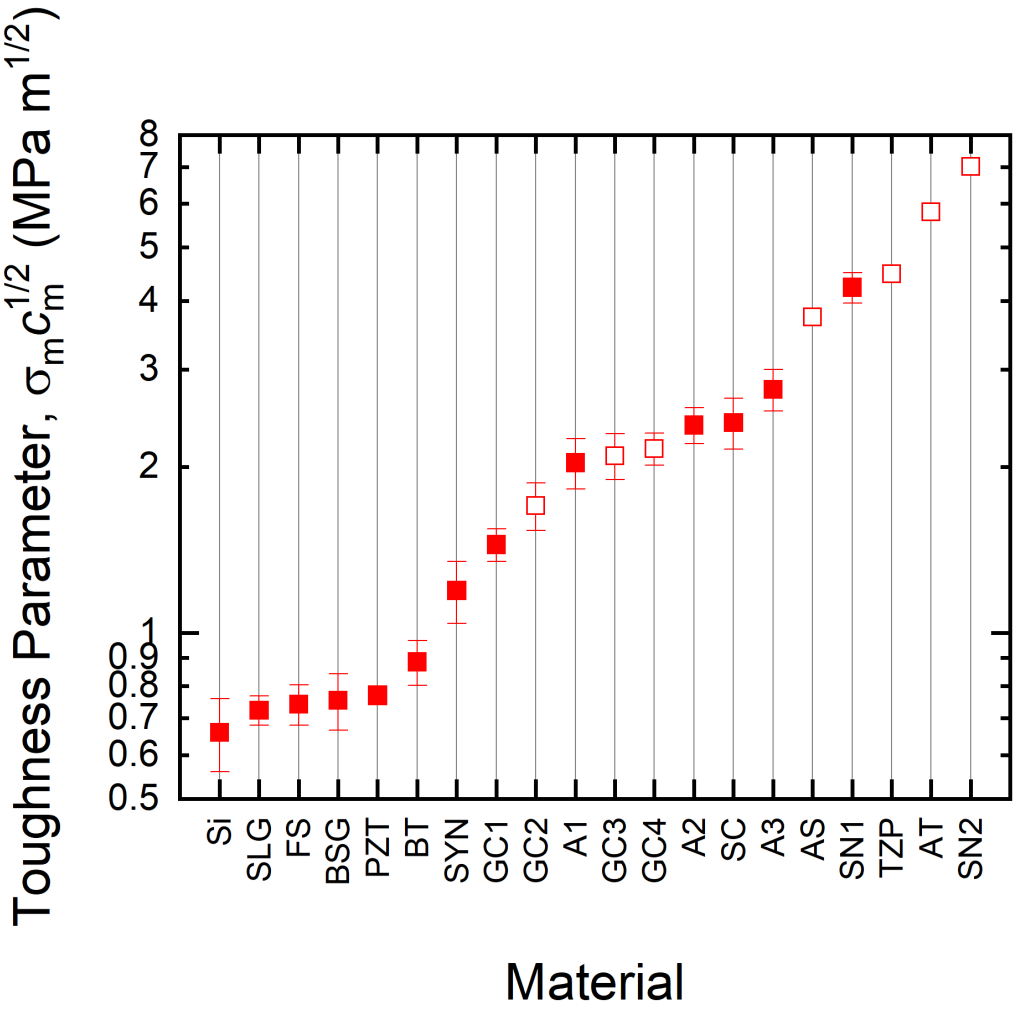

FIGURE 3 Plot of ranked toughness parameter, $\sigma_m c_m^{1/2}$, for ceramic materials. The solid symbols represent materials with single valued toughness. The open symbols represent the upper bound toughness values for materials exhibiting T curves. Tougher materials on right.

Table 2 Ceramic toughness parameters

Material, *P* (N)	$\sigma_m P^{1/3}$ (MPa $N^{1/3}$)	$c_m P^{-2/3}$ (μm $N^{-2/3}$)	$\sigma_m c_m^{1/2}$ (MPa $m^{1/2}$)
Si, 2–50 N	133±6 (75)	26.6±5.1 (20)	0.66±0.10
SLG, 0.1–10 N	137±8 (87)	27.9±1.2 (40)	0.72±0.04
FS, 5–50 N	190±12 (40)	15.2±2.7 (21)	0.74±0.06
BSG, 5–100 N	173±19 (129)	19.0±2.2 (35)	0.75±0.09
PZT, 10 N	126±4	37.4±3.7 (24)	0.77±0.03
BT, 10 N	183±16	23.4±3.0 (24)	0.89±0.08
SYN, 100 N	281±34	18.0±2.8 (16)	1.2±0.2
GC1, 20 N	396±16	13.3±2.0 (22)	1.4±0.1
GC2, 100 N*	361±10* (12)	21.6±4.3* (8)	1.7±0.2*
A1, 5 N	608±54	11.2±1.6 (21)	2.0±0.2
GC3, 100 N*	440±25* (11)	22.7±3.5* (8)	2.1±0.2*
GC4, 100 N*	512±18* (8)	17.7±2.0* (8)	2.2±0.1*
A2, 20 N	711±36	11.2±1.5 (36)	2.4±0.2
SC, 10 N	747±57	10.4±2.3 (22)	2.4±0.3
A3, 10-200 N	561±40	24.3±2.4 (8)	2.8±0.2
AS, 322 N*	993*	14.2*	3.7*
SN1, 20, 50 N	1045±55	16.4±0.7 (6)	4.2±0.3
TZP, 300 N*	1666*	13.3*	4.5*
AT, 300 N*	876*	43.6*	5.8*
SN2, 374 N*	2009*	12.2*	7.0*

3.3. Application of modified technique

For materials that exhibit load-dependent $\sigma_m P^{1/3}$ and $c_m P^{-2/3}$ values, it is a simple extension of the above analysis to show that using P as a parameter enables the T curve to be determined via generalization of Eq. (6) [Braun, 1992; Cook, 2015]:

$$T(c) = (4\psi/3)\sigma_m(P)c_m^{1/2}(P). \quad (8)$$

Two applications of the modified indentation toughness technique using Eq. (8) are demonstrated here. The first application considers microstructural alteration of the family of lithium silicate glass ceramics, GC2, GC3, and GC4 and development of the resulting T curves. These are moderately tough ceramics with short T curves. The second application considers the variation in the T curves of four engineered polycrystalline ceramics, AS, AT, SN2, and TZP. These are regarded as very tough ceramics with long T curves. For convenience, the geometry parameter will be taken here as $(4\psi/3) = 1$.

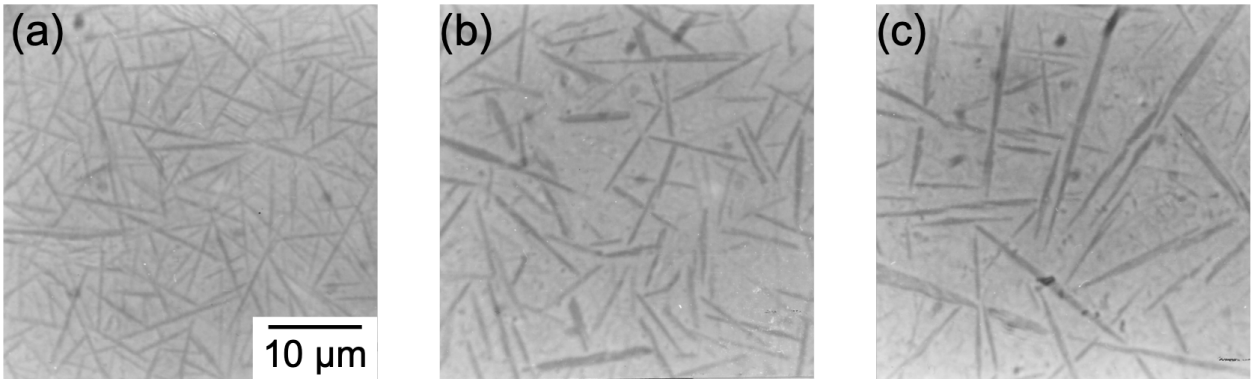

FIGURE 4 Optical micrographs of the (a) GC2, (b) GC3, and (c) GC4 glass-ceramic materials. (Note that material IDs are different from those used earlier [Cook *et al.*, 1986; Cook, 2020].)

Figure 4 is a set of optical micrographs of the GC2, GC3, and GC4 materials. The light contrast major matrix phase is cristobalite and the dark contrast minor platelet phase is Li_2SiO_3. Both the platelet size and the mean free path in the major phase increase in order GC2, GC3, GC4. Detailed microstructural morphology and compositional information is given elsewhere [Cook *et al.*, 1986], but it is clear that the materials represent a set of microstructures of increasing scale. Fracture instability data over the indentation load domain P = 2–100 N were

obtained for the three materials by application of the dummy crack method in dry N_2 gas. Approximately 12 measurements were performed at each load. Figure 5(a) is a logarithmic plot of $T(c)$ determined from these data and application of Eq. (8). The symbols represent the mean values obtained at each load and the bars represent the uncertainty determined from the experimental standard deviations and propagation of variance at each load. The symbols at the longest crack length for each material reflect the data in Table 2. The lines are guides to the eye.

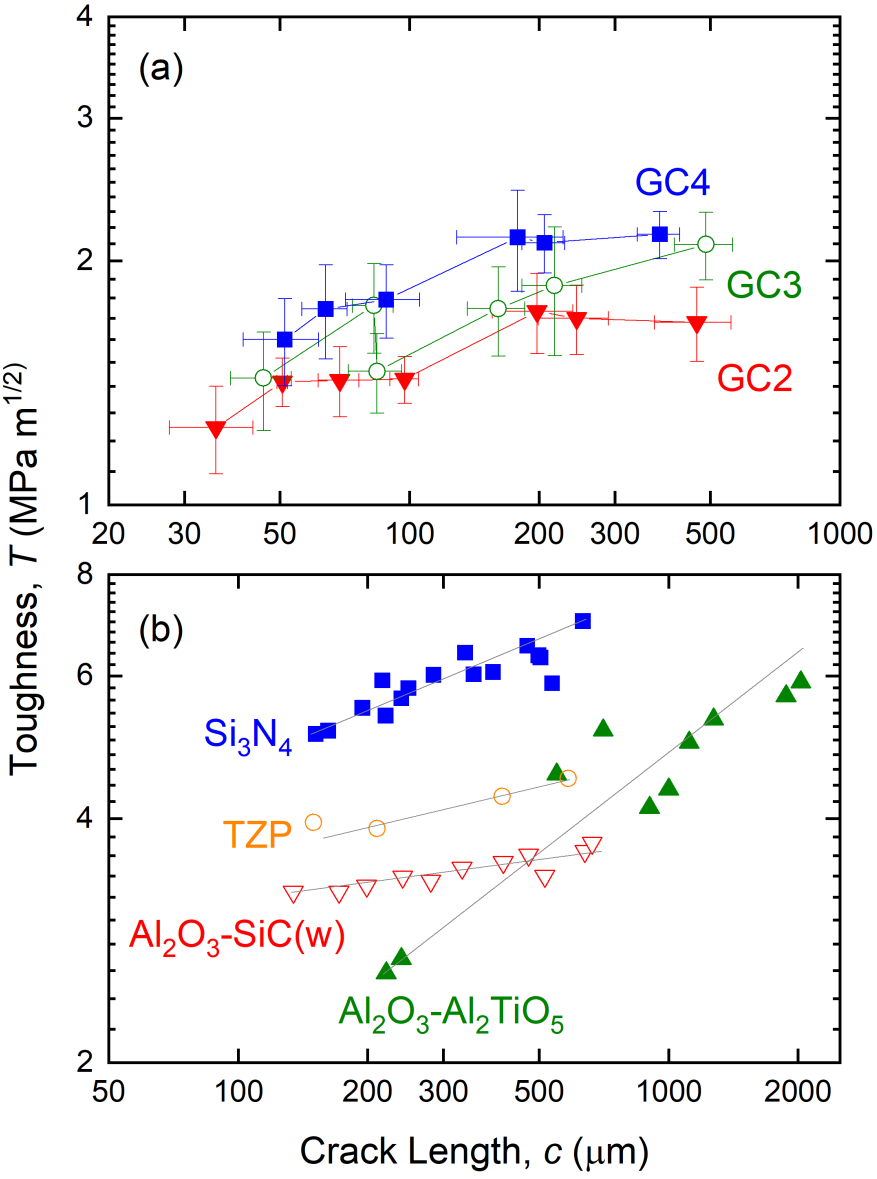

FIGURE 5 Variations in toughness with crack length, T curves $T(c)$, for (a) a set of glass ceramics with related microstructures and (b) a group of ceramics with different toughening mechanisms. Data obtained using modified indentation toughness technique.

It is clear from Fig. 5(a) that these materials exhibit T curves. For the set of materials, the toughness increases within a crack length domain of 30 μm to 500 μm over a range of approximately 1.2–1.6 MPa $m^{1/2}$ to approximately 1.7–2.3 MPa $m^{1/2}$. Larger microstructural scales exhibited greater toughness values at all crack lengths in the order GC2, GC3, GC4. There was a slight tendency to toughness plateaux at crack lengths longer than approximately 200 μm. Observations of crack extension in these materials showed that microstructurally-induced frictional interlocks and ligamentary bridges formed in the crack wakes, leading to cohesive traction zones [Braun, 1992; Cook, 2015]. Specifically, the platelets appeared more fracture resistant than the matrix, leading to the necessary crack deflection and discontinuous crack propagation required for interlock and bridge formation. The implication of Fig. 5(a) is that the effects of the cohesive zones, but not necessarily the length scales, increased with the scale of the microstructure. Although detailed discussions of toughening mechanisms are beyond the scope of this work, it is clear that a multitude of platelet-related elements, of order 10 μm in scale, Fig. 4, must be responsible for the observed toughness variations over approximately 100 μm in scale, Fig. 5(a). Such toughness variations could not be discerned by large fracture specimens that typically involve cracks tens of millimeters in length and only sense plateau toughness responses.

Figure 5(b) shows the T curves for four deliberately toughened materials, using a logarithmic plot with relative dimensions identical to Fig. 5(a). The $T(c)$ variations were determined by analyses of published load-dependent indentation fracture data obtained using peak load domains extending to approximately 300 N [Ramachandran and Shetty, 1991; Braun *et al*., 1992; Li *et al*., 1997]. The symbols represent toughness values calculated from application of Eq. (8) to individual σ_m-c_m pairs measured at each load. As above, the symbols at the longest crack lengths reflect the data in Table 2 and the lines are guides to the eye. Three of the materials in Fig. 5(b) were engineered to exhibit crack wake cohesive traction zones with the necessary crack deflections and formation of frictional interlocks and ligamentary bridges: (i) Si_3N_4 contains elongated grains in a fine-grained matrix; (ii) Al_2O_3-SiC (w) is a composite of a fined grained alumina matrix containing tough SiC whiskers; and (iii) Al_2O_3-Al_2TiO_5 is a composite of an alumina matrix containing aluminum titanate particles—the particles are thermally mismatched

with the matrix leading to an inhomogeneous internal stress field. The fourth material in Fig. 5(b) is yttria stabilized tetragonal zirconia polycrystal and was engineered to exhibit energy consuming phase transformations triggered by crack front stress fields (the monoclinic phase is stable at ambient conditions and dilates and shears on transformation).

There are several clear differences between the T curves of Fig. 5(a) and 5(b). First, the toughness and crack length scales required to plot the responses of the materials in Fig. 5(b) are approximately a factor of two greater, highlighting the greater load-bearing capacity of these more fracture resistant materials. Second, the range of toughness values, approximately 2 MPa $m^{1/2}$ to 7 MPa $m^{1/2}$, is much greater for the group of materials in Fig. 5(b), indicative of the different materials families represented. Third, with one exception, the responses of individual materials in Fig. 5(b) exhibit somewhat weaker relative increases of toughness with crack length, although, fourth, the materials in Fig. 5(b) do not exhibit tendencies to plateau toughness values at long crack lengths. Again, such toughness variations could not be discerned by large, long crack fracture specimens.

4. DISCUSSION

Significant extensions to a modified indentation technique for toughness determination of ceramics and other brittle materials have been provided here. The extensions refine the earlier work [Cook and Lawn, 1983] by examining more materials, acquiring new data, including data from other investigators and other techniques [Marshall, 1983; Ramachandran and Shetty, 1991; Braun *et al*., 1992; Li *et al*., 1997], and re-analysing raw data to better assess uncertainty. As a consequence, the technique can be used with greater confidence in both materials engineering applications and materials science investigations. In particular, for materials engineering, a major new result is the ranking of materials by a direct output of the technique, the toughness parameter $\sigma_m c_m^{1/2}$. The ranking generated here, Fig. 3, provides a clear foundation and design tool for assessing the relative merits of materials in development and for materials selection. In addition, the level of uncertainty exhibited by the current materials within the ranking provides a quantitative basis for assessing the accuracy and precision of measurements on new materials.

Importantly, the ranking is based on the toughness characteristics of materials at length scales relevant to strength-controlling flaws.

As a design tool, implementation of the modified indentation toughness technique requires a little more effort than conventional indentation toughness assessment methods [Anstis *et al*., 1981; Chantikul *et al.,* 1981], but exactly the same effort as common long-crack toughness measurements using standard fracture mechanics specimens [Murakami, 1987]. Both modified indentation and standard specimen measurements are based on sound fracture mechanics, both require the creation and measurement of carefully controlled cracks in specimens of known geometry, and both require measurement of the peak sustainable load or stress of the specimen. The long cracks of standard specimen geometries practically eliminate dependence of toughness assessment on the mechanism by which the cracks were initiated and formed. The indentation strength method [Chantikul *et al.,* 1981] significantly reduces dependence on the crack initiation and formation mechanism relative to the indentation crack length method [Anstis *et al*., 1981], but a weak dependence remains. The modified technique removes this dependence completely, reducing the uncertainty in toughness assessment to that associated with crack geometry, similar to that for long crack measurements. As a consequence of reduced influence of the indentation residual field in application of the modified technique, the materials rankings are considerably different from those arising from conventional crack length measurements $c_{\text{air}}P^{-2/3}$ alone (Fig. 2) and slightly different from strength measurements $\sigma_{\text{m}}P^{1/3}$ alone (Table 2).

From a materials science perspective, a major new result is the application of the modified indentation toughness technique to determine T curves, $T(c)$, Fig. 5. Such determination enables the establishment of structure-properties relations for materials that exhibit microstructural influences on crack propagation. For example, the larger microstructural scale of the GC4 material is correlated with a greater long crack, steady-state toughness, Fig. 5(a), whereas the short crack toughness values of GC2, GC3, and GC4 appear to be similar. The implication is that fracture in the matrix of all three glass-ceramics is similar but that larger platelets cause greater energy dissipation during crack extension. Similarly, the enhanced toughness and toughness increase with crack length for Si_3N_4 relative to Al_2O_3-SiC(w) in Fig. 5(b) suggests that elongated Si_3N_4 grains are more potent cumulative toughening agents at longer crack length scales than

SiC(w) in Al_2O_3. Such observations enable materials science based models of toughening at strength relevant length scales to be developed. (It is noted that some of the T curves reported here differ somewhat from those published earlier [Ramachandran and Shetty, 1991; Braun *et al*., 1992; Li *et al*., 1997]. This is simply a consequence of slightly different numerical factors used in analysis.)

Finally, another materials science insight comes from interpretation of the apparently small value of $T_{air}/T_0 \simeq 0.4$. This small value was implied by crack lengths observed in air after indentation relative to those at crack instability in inert conditions under applied stress (section 3.1.). For simplicity, the same residual field geometry factor, χ_{air}, was implemented in the strength analysis, Eqs. (3) and (5), leading to elimination of this factor on comparison of the initial and final crack lengths, Eq. (7). As a consequence, interpretation of the relative crack lengths was made solely in terms of relative toughness values in air and inert conditions, with implications for the chemical reduction of ceramic surface energies on exposure to moisture. The small value of T_{air}/T_0 suggests much greater reduction than more detailed experiments in water imply [Cook, 2015]; $T_{water}/T_0 \simeq 0.7$, placing a lower bound on T_{air}. The resolution to this discrepancy lies in recognizing that the residual field geometry term is changed under the action of applied stress such that $\chi = \chi_{stress}$ in Eqs. (3) and (5), and Eq, (7) becomes

$$c_m/c_{air} = (4\chi_{stress}T_{air}/\chi_{air}T_0)^{2/3}. \quad (8)$$

The implication from the combined observations and Eq. (8) is that the effect of the residual field is reduced significantly on application of stress to an indentation flaw, such that $\chi_{stress}/\chi_{air} \simeq 0.5$. This reduction has wide materials science implications for the behavior of contact flaws under stress.

5. CONCLUSIONS

Additional measurements and comparisons affirm that the modified indentation toughness technique provides an accurate and precise method for qualitative ranking and quantitative determination of ceramic toughness. The method is applicable to materials that exhibit variations in toughness with crack length, T curves. The modified technique has much in common with

standard long crack measurement methods in that a load or stress and crack length at specimen instability are combined to assess material toughness. However, the modified technique has the advantages of ease of indentation crack formation and placement and measurement of material toughness at length scales relevant to strengths of structural ceramics. The artifacts associated with sole use of indentation crack length or indentation strength measurements, particularly for glasses, are largely removed by the modified technique with little additional experimental effort.

REFERENCES

Anstis GR, Chantikul P, Lawn BR, Marshall DB (1981) A critical evaluation of indentation techniques for measuring fracture toughness: I, Direct crack measurements. J Am Ceram Soc 64:533–538.

Bennison SJ, Padture NP, Runyan JL, Lawn BR (1991) Flaw-insensitive ceramics. Phil Mag Letters 64:191–195.

Braun LM, Bennison SJ, Lawn BR (1992) Objective evaluation of short−crack toughness curves using indentation flaws: Case study on alumina−based ceramics. J Am Ceram Soc 75:3049–3057.

Chantikul P, Anstis GR, Lawn BR, Marshall DB (1981) A critical evaluation of indentation techniques for measuring fracture toughness: II, Strength method. J Am Ceram Soc 64:539–543.

Chantikul P, Bennison SJ, Lawn BR (1990) Role of grain size in the strength and R−curve properties of alumina. J Am Ceram Soc 73:2419–2427.

Cook RF (2006) Strength and sharp contact fracture of silicon. J Mater Sci 41:841-872.

Cook RF (2015) Multi-scale effects in the strength of ceramics. J Am Ceram Soc 98:2933–2947.

Cook RF (2019) Fracture sequences during elastic-plastic indentation of brittle materials. J Mater Res 34:1633–1644.

Cook RF (2020) A critical evaluation of indentation crack lengths in air. J Am Ceram Soc 103:2278–2295.

Cook RF, Lawn BR (1983) A modified indentation toughness technique. J Am Ceram Soc 66:C200–C201.

Cook RF, Freiman SW, Baker TL (1986) Effect of microstructure on reliability predictions for glass-ceramics. Mater Sci Eng A 77:199–212.

Dabbs TP (1984) Fatigue properties of high strength glass with particular reference to optical fibers. Ph.D. Thesis. University of New South Wales, Kensington, Australia.

Dabbs TP, Lawn BR, Kelly PL (1982). A dynamic fatigue study of soda-lime silicate and borosilicate glasses using small scale indentation flaws. Physics Chemistry Glasses, 23:58–66.

Li J-F, Kawasaki A, Watanabe R (1997) R-curve determination of 3Y-PSZ by the indentation strength-in-bending method. J Ceram Soc Japan 105:88–90.

Marshall DB (1983) Controlled flaws in ceramics: A comparison of Knoop and Vickers indentation.J Am Ceram Soc 66:127–131.

Ramachandran N, Shetty DK (1991) Rising crack-growth-resistance (R-curve] behavior of toughened alumina and silicon nitride. J Am Ceram Soc 74:2634–2641.

Stress intensity factors handbook. Murakami Y ed. Oxford, UK: Pergamon Press, 1987.